5. Conclusion

To summarize, we have shown that two types of excited charge-transfer states, the TICT states and the exciplexes, behave similarly in that they exhibit an unusual temperature dependence of their emission rate constant k_f which can be described in both cases by vibrational activation. For the nonactivated molecule, i.e., for the equilibrium structure of the excited state, the transition moment $\vec{M}$ has a very low value (minimum) corresponding to the forbidden radiative back electron transfer[44] and rises more or less steeply upon deformation through vibrational activation. The activation energy of k_f constitutes, in principle, a valuable tool to characterize the type of vibration involved. It can also serve to characterize solvent effects. While for the TICT states a minimum for M is clearly predicted for the perpendicular geometry from orbital overlap considerations, the situation in the exciplexes and especially intramolecular exciplexes is less straightforward. If the complex is symmetric with the nitrogen above the center of mass of the aromatic moiety, it will always have a C_{2v} or a C_{6v} symmetry. This geometry will always correspond to an extreme value of the orbital overlap and the Coulomb attraction. As in the systems considered here the HOMO and the LUMO of the donor are symmetric ($2p_N$ and $3s_N$), nonzero overlap is only possible with a symmetric orbital of the acceptor (i.e., one with no nodal plane perpendicular to the aromatic acceptor system). As this orbital is never involved in exciplex formation, the most symmetric exciplex geometry will correspond to zero orbital overlap for the systems considered here.

If the Coulomb attraction is a maximum for the symmetric geometry, this will also correspond to the most stable exciplex geometry. When the amino group is not hindered by the chain, its position in the exciplex will be that corresponding to the largest Coulomb attraction and therefore also correspond to zero orbital overlap. In this situation the temperature dependence of k_{fE} will mainly be a first-order effect.

However, when the alkyl chain prevents the attainment of this geometry the Coulomb attraction and the symmetry of the exciplex will be decreased. In this case the temperature dependence of the fluorescence rate constant will mainly be a second-order effect.

Contrary to TICT state forming molecules, the exciplex geometry is mainly determined by the balance between the Coulomb attraction and nonbonded interactions. On the one hand, these two factors depend much more strongly on the geometry of the exciplex than in the TICT forming molecules where the rotation around the carbon nitrogen bond in the vicinity of $\phi = 90°$ leads only to minor changes of Coulomb attraction and nonbonded interactions. On the other hand, the small atomic overlap integrals, caused by the larger distance (2.5–3 Å) between the atomic orbitals of donor and acceptor, lead to a much smaller interaction between the zeroth-order ground state and the charge-transfer state for symmetry-disturbed exciplex geometries as compared to off-perpendicular TICT geometries.

The changes of the wave functions of the TICT states and of the exciplexes should be reflected in some temperature dependence of the corresponding transient absorption spectra. These spectra, usually consisting of several transitions of different nature,[45] are expected to simplify at lower temperatures. In the case of the symmetry or/and overlap-forbidden pure CT states, the transient absorption spectra would correspond to the sum of the nearly pure local transitions in the radical ion subunits, D^+ and A^- (as in ref 11). Such study has not yet been done.

Similar exceptions to the general rule, i.e., the emission rates being thermally activated, are expected to be found in other flexible molecules or molecular complexes, wherever the luminescent transition from the equilibrium excited state would be highly forbidden.

Acknowledgment. M.V.d.A. is a research associate of the Belgian National Science Foundation and thanks the Belgian National Science Foundation and the Ministry for Scientific Programmation for Financial Support. W.R. thanks the Deutsche Forschungsgemeinschaft for financial support and a Heisenberg fellowship. The lifetime measurements at BESSY were made possible through support from the Bundesministerium für Forschung und Technologie (project 05 314 FAI). Part of this work was done under Polish Project CPBP 1.19.

(44) Grabowski, Z. R. In *Supramolecular Photochemistry*; Balzani, V., Ed.; D. Reidel: Dordrecht, 1987; p 319.

(45) Potashnik, R.; Goldschmidt, C. R.; Ottolenghi, M.; Weller, A. *J. Chem. Phys.* **1971**, *55*, 5344.

Mesophases and Crystalline Phases in Fatty Acid Monolayers†

R. M. Kenn,* C. Böhm, A. M. Bibo, I. R. Peterson, H. Möhwald,

Institut für physikalische Chemie, Universität Mainz, Welder-Weg 11, D6500 Mainz, FRG

J. Als-Nielsen, and K. Kjaer

Physics Department, Risø National Laboratory, DK4000 Roskilde, Denmark *(Received: July 2, 1990)*

The polymorphism in docosanoic (behenic) acid monolayers at the air/water interface is investigated by means of X-ray diffraction. Analysis of the diffraction spot profiles parallel and perpendicular to the surface provides detailed data on the unit cells of five different phases (L_2, L_2', S, CS, and LS) with uniform aliphatic tail alignment and regular two-dimensional lattice structure. The first four of these display centered rectangular symmetry, while the LS phase is hexagonal. In the LS, S, and CS phases the tails are oriented normal to the surface, whereas in L_2 and L_2' they are tilted toward the nearest and next-nearest neighbors, respectively. The unit cells of the S and CS phases have the same symmetry. However, the latter is the only phase to display the packing density (<0.19 nm^2 aliphatic chain cross section), the very low compressibility (<3 × 10^{-4} m/mN), and the resolution-limited peak width (<0.03 nm^{-1}, corresponding to a characteristic length for exponential decay of positional correlations equal to more than 160 lattice spacings) expected from a close-packed crystalline solid. In contrast, the peak width in the L_2, L_2', LS, and S phases is more than 0.09 nm^{-1}, corresponding to a correlation length of less than 54 lattice spacings. Their similarities to mesophases of liquid crystals are pointed out.

Introduction

Monolayers of fatty acids have been studied intensively for many years[1] but are still far from being understood. This is unfortunate, since they are arguably the simplest surfactants and are well suited as models for the theoretical calculation of the arrangement and conformation of molecules at interfaces.[2-5] Fatty acids are also

† Dedicated to Prof. A. Weller on the occasion of his retirement.

(1) Pockels, A. *Nature* **1891**, *43*, 437.

0022-3654/91/2095-2092$02.50/0

the surfactants most widely used for preparing Langmuir–Blodgett films.[6] It has been demonstrated that these films are suitable for a variety of applications, but many of these depend on the fabrication of nearly perfect films, which in turn necessitates understanding and control of their microstructure.[7]

It has been shown that the structure of a monolayer may be controlled by manipulating it at the air/water interface.[7] At this stage the molecules are quite mobile and possess many degrees of freedom which can be influenced. On the other hand, there is a lack of suitable techniques that yield direct information on film microstructure. Important progress has been achieved by the introduction of synchrotron X-ray techniques to study monolayers on water surfaces. By measuring the specular reflectivity at the interface as a function of incidence angle it is possible to determine the electron density distribution along the surface normal, and hence film parameters such as thicknesses and densities of hydrophobic and hydrophilic regions and surface roughness.[8] In-plane diffraction of the evanescent X-ray beam generated at the interface when the incoming beam is incident below the critical angle yields the periodic molecular arrangement within the film plane.[9,10]

In the present in-plane diffraction study, the Bragg rod profiles have been measured with high resolution in directions parallel and perpendicular to the surface. This yields accurate data on the positional coherence and on the orientation of aliphatic tails with respect to the surface normal. We have concentrated on docosanoic (behenic) acid ($CH_3(CH_2)_{18}COOH$), since previous isotherm measurements with the straight-chain fatty acids have shown that much of the polymorphism encountered in the homologous series is conveniently accessible with this member. The existence of different structures is revealed, and we also discuss to what extent the data can be generalized.

Experimental Section

Docosanoic acid (>99.5% pure) was purchased from Fluka, Buchs, CH, and the water used was Millipore filtered. P.A. grade chloroform (Merck) was used as spreading solvent. Π–A isotherms were measured by using a Lauda film balance at a compression and expansion rate of 50 $pm^2\ s^{-1}$ [11] and were used to establish the Π–A–T phase diagram.

For the synchrotron X-ray diffraction studies a dedicated film balance was placed at the sample stage of the D4 diffractometer at HASYLAB, DESY, Hamburg, FRG.[12] Due to long-term drifts, the accuracy in measurement of the absolute value of the surface pressure was not better than 3 mN/m. In addition, the temperature could not be measured more accurately than ±3 °C, especially at the lowest temperatures investigated. However, during the synchrotron runs the isotherms were measured sufficiently precisely to locate phase transitions, so that there is no uncertainty about which phase of Figure 2 caused each of the distinct X-ray diffraction patterns.

In all the X-ray measurements, the synchrotron beam was monochromated to a wavelength $\lambda = 0.138$ nm by Bragg reflection from a Ge(111) crystal and was adjusted to hit the surface an an incident angle $\alpha \simeq 0.116° = 0.85\alpha_c$ where $\alpha_c = 0.137°$ is the critical angle for total external reflection.[13] The resulting evanescent X-ray beam penetrates less than 10 nm below the surface and is diffracted by the internal structure in the monolayer. The resulting Bragg rod profiles were measured by using a vertically mounted position-sensitive detector (OED100M, Braun, Garching, FRG). The detector accepted photons over a range $-0.16 < Q_z < 9\ nm^{-1}$, where $Q_z = (2\pi/\lambda)\sin\alpha_F$ is the out-of-plane component of the scattering vector, α_F being the detector elevation angle. Its vertical fwhm resolution was 0.049 nm^{-1}. A Soller collimator provided a resolution of 0.07 nm^{-1} of Q_x, the in-plane component of the scattering vector; $Q_x \simeq (4\pi/\lambda)\sin\theta$, 2θ is the horizontal diffraction angle.

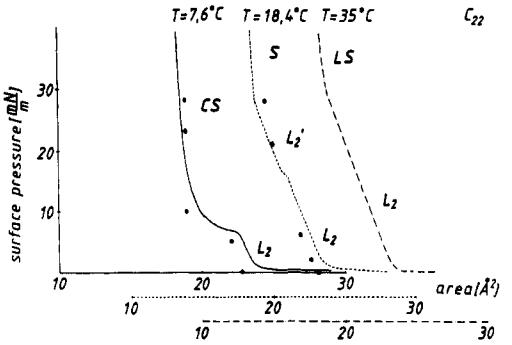

Figure 1. Surface pressure as a function of molecular area for docosanoic acid monolayers at different temperatures. The abcissae corresponding to the three temperatures are shifted for clarity. The points show the values *for molecular area* A_t derived from the present X-ray data.

Two types of measurement of the scattered radiation were made. In the first, the Q_x scans, the detector counts were not resolved in Q_z, so that the total count represents the integral of scattered intensity along a vertical Bragg rod. In the second, the Q_z-resolved scans, the counts from each Q_z interval were accumulated separately in a multichannel analyser. Because of measurement time limitations, Q_z-resolved measurements were only performed for those values of Q_x corresponding to peaks of the Q_x intensity measurements, and for nearby Q_x values in order to determine the background.

Two types of information were extracted from the measured profiles. Firstly, the peaks of the Q_x scans were assumed to be power-pattern Bragg peaks of a two-dimensional lattice, and the position of a peak center $Q_{x,pk}^{hk}$ was converted into d spacings by using the Bragg formula:

$$d_{hk} = 2\pi/Q_{x,pk}^{hk} \quad (1)$$

The positional correlation length ξ for each Q_x-scan peak was calculated from its full width at half-maximum (fwhm, corrected for resolution effects) assuming exponential decay of positional correlations with increasing separation within the layer:

$$\xi = 2/\mathrm{fwhm}(Q_x) \quad (2)$$

Secondly, information about the orientation of the molecules was extracted from the Q_z-resolved scans, assuming that the aliphatic tails are uniformly tilted. The angle t between molecular axis and surface normal is then given by the formula[13]

$$\tan(t)\cos(\Psi_{hk}) = Q_{z,pk}^{hk}/Q_{x,pk}^{hk} \quad (3)$$

where $Q_{z,pk}^{hk}$ is the position of the peak along the Bragg rod, $Q_{x,pk}^{hk}$ is the Q_x-peak position, and Ψ_{hk} is the azimuthal angle between the tilt direction projected on the surface and the reciprocal lattice vector corresponding to the reflection $\{h,k\}$.

Hence the molecules are perpendicular to the water surface if and only if all values of $Q_{z,pk}^{hk}$ are zero.

(2) Baremann, J. P.; Gardini, G.; Klein, M. L. *Phys. Rev. Lett.* **1988**, *60*, 2152.
(3) Popielawski, J.; Rice, S. A. *J. Chem. Phys.* **1988**, *88*, 2.
(4) Harris, J.; Rice, S. A. *J. Chem. Phys.* **1989**, *91*, 4994.
(5) Cantor, R. S.; McIlroy, P. M. *J. Chem. Phys.* **1989**, *90*, 4423.
(6) Roberts, G. G. *Adv. Phys.* **1985**, *34*, 475.
(7) Peterson, I. R. *J. Chim. Phys.* **1988**, *85*, 997.
(8) Helm, C. A.; Möhwald, H.; Kjaer, K.; Als-Nielsen, J. *Europhys. Lett.* **1987**, *4*, 697.
(9) Kjaer, K.; Als-Nielsen, J.; Helm, C. A.; Laxhuber, L. A.; Möhwald, H. *Phys. Rev. Lett.* **1987**, *58*, 2224.
(10) Dutta, P.; Peng, J. B.; Lin, B.; Ketterson, J. B.; Prakash, M.; Georgopoulos, P.; Ehrlich, S. *Phys. Rev. Lett.* **1987**, *58*, 2228.
(11) Bibo, A. M.; Knobler, C. M.; Peterson, I. R. *J. Phys. Chem.*, submitted for publication.
(12) Helm, C. A.; Möhwald, H.; Kjaer, K.; Als-Nielsen, J. *Biophys. J.* **1987**, *52*, 381.
(13) Als-Nielsen, J.; Kjaer, K. In *Phase Transitions in Soft Condensed Mater*; Riste, T., Sherrington, D., Eds.; NATO ASI Series B; Plenum: New York, 1989; Vol. 211, pp 113–138.

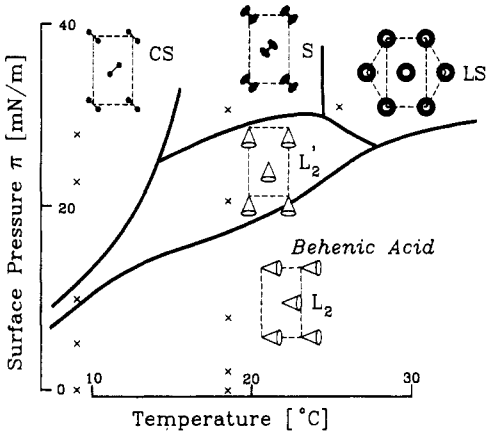

Figure 2. Phase diagram of docosanoic acid as deduced from isotherm measurements. The symbols used for the different phases are taken from ref 16. The crosses indicate the surface conditions for the X-ray diffraction measurements of Figure 3. The inserts show for each phase the structure deduced from the X-ray measurements (cf. below).

Results and Interpretation

Figure 1 shows the surface pressure Π as a function of molecular area A for docosanoic acid at three different temperatures. At the lowest temperature (7.6 °C), the dominant feature is a broad, nearly horizontal region joining two nearly vertical lines. This is consistent with a first-order phase transition into a phase with an average molecular area of approximately 0.18 nm^2/molecule, very close to the cross section of 0.1835 nm^2 observed in the densest known crystalline packings.[14] The intermediate curve at room temperature displays more subtle changes in slope, revealing the existence of more than one phase transition. At the highest temperature (35 °C), the isotherm resembles that of eicosanoic (arachidic) acid at room temperature.[15] There are three essentially linear regions of very different compressibility with breakpoints near molecular areas A of 0.24 and 0.20 nm^2, respectively.

The data for the Π–T phase diagram of Figure 2 were obtained from a series of isotherm measurements.[15] It is basically in accordance with the diagram of Ställberg-Stenhagen and Stenhagen[16] and uses their symbols for the different phases. It is the aim of the present work to characterize these phases. We have obtained detailed data on phases L_2, L_2', S, CS, and LS.

Figure 3a shows the Q_x scans at 7 °C for several different surface pressures. The asymmetry of the profile at low pressures hints at the presence of two unresolved lines. At higher pressures, the diffraction pattern changes abruptly with the appearance of two sharp well-resolved lines typical for a crystalline solid. Also as expected for a crystalline solid, the positions of these peaks do not change significantly with pressure. The 18.5 °C Q_z scans of Figure 3b show different film behavior. Even at a surface pressure of less than 1 mN/m two rather broad peaks of different widths are resolved. The center positions move outwards on compression to a much greater extent than occurs in Figure 3a for the CS phase, indicating a higher compressibility. The narrower and broader peaks cross over at 8 mN/m. The width of the narrower peak does not vary markedly on compression and corresponds to a coherence length smaller than in CS. There appear to be no abrupt changes in the profiles corresponding to transitions between the three different phases L_2 (0, 2, and 8 mN/m), L_2' (21 mN/m), and S (31 mN/m) covered in the figure. However, differences between the phases are visible in the Q_z-resolved Bragg rod scans of Figure 4, which shows Q_z profiles for both peaks of the Q_x scans, for four distinct conditions, each corresponding to a distinct phase. In phase L_2, the broader peak of the Q_x scan exhibits a Q_z-resolved maximum for $Q_z > 0$. The second, Q_z-resolved scan peaks at Q_z

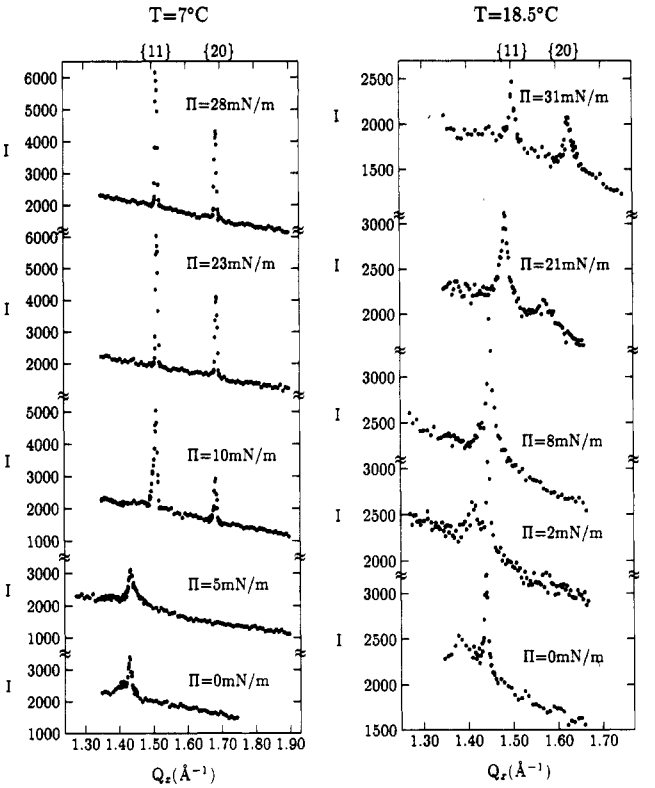

Figure 3. Q_x scans of X-ray scattering intensity as a function of the in-plane component Q_x of scattering vector for docosanoic acid monolayers at (a) 7 °C and (b) 18.5 °C and at the surface pressures indicated. In each case the {11} peak lies to the left of the (20) peak.

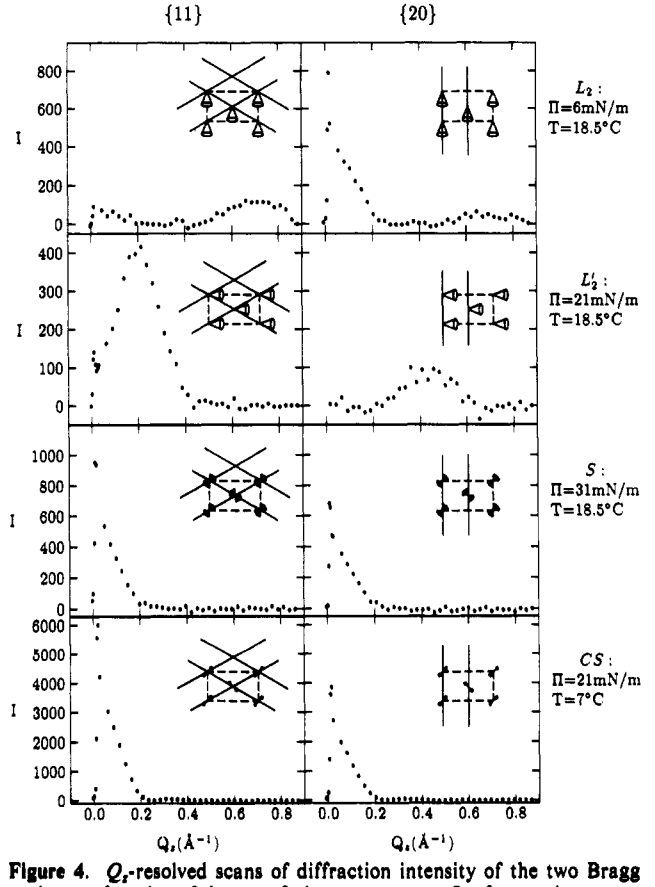

Figure 4. Q_z-resolved scans of diffraction intensity of the two Bragg peaks as a function of the out-of-plane component Q_z of scattering vector for docosanoic acid monolayers in the four different phases appearing in Figure 3. The two-dimensional lattice (dashed lines) and the projection of the tilt direction (cones) are also given (for the L_2 and L_2' phases), as well as the diffracting {11} or (20) lines.

(14) Ewen, B.; Strobl, G. R.; Richter, D. *Faraday Discuss.* **1980**, *69*, 19.
(15) Bibo, A. M.; Peterson, I. R. *Adv. Mater.* **1990**, *2*, 309.
(16) Ställberg-Stenhagen, S.; Stenhagen, E. *Nature* **1945**, *156*, 239.

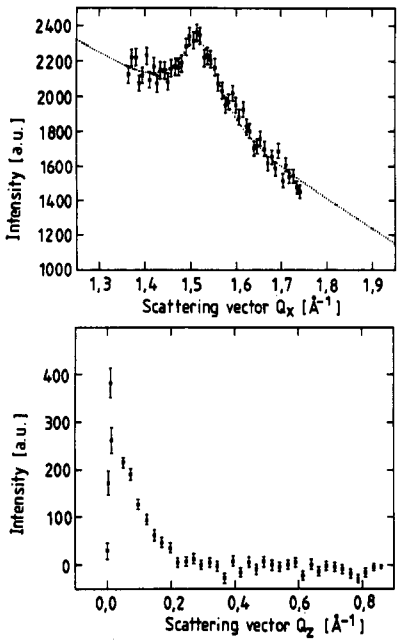

Figure 5. Scattered intensity scans for docosanoic acid monolayers in the LS phase at 25 °C and 30 mN/m: (a, top) Q_z-integrated and (b, bottom) Q_z-resolved.

= 0, and in addition shows indications of a second maximum with much lower intensity, which may be identified as the tail of the broader reflection. In phase L_2', both values of $Q_{z,pk}^{hk}$ are nonzero and are in the ratio 2:1, with larger $Q_{z,pk}^{hk}$ corresponding to larger $Q_{z,pk}^{hk}$. For phases S and CS, on the other hand, both peaks exhibit a maximum for $Q_z = 0$.

Figure 5 shows the measurements made for the LS phase. The Q_x scan in Figure 5a shows only one peak, considerably broader than that measured for the other phases. Figure 5b gives the corresponding Q_z-resolved scan, whose maximum occurs for zero Q_z.

The interpretation of these rod scans is rather straightforward. In all known 3D packings of aliphatic chain derivatives (alkanes, carboxylic acids, alcohols, etc.), the molecules are packed in layers.[17] Each molecule is surrounded by six nearest neighbors in the layer, forming a hexagon which is usually slightly distorted from regularity. A general packing of this type gives rise to three reflections of lowest order. The fact that only two are observed in the L_2, L_2', S, and CS two-dimensional phases means that two of these are degenerate, and points to a rectangular packing, either centered or primitive, in which the (11) and (1$\bar{1}$) reflections are degenerate but the (20) reflection remains distinct. In the LS phase all three reflections are degenerate, indicating hexagonal symmetry.

In phase L_2 the chains are tilted toward a nearest neighbor along the short [01] side of the unit-cell rectangle. Since they are normal to the longer [10] unit-cell vector but not to any other in-plane vector, only the Q_z-resolved scan for the (20) peak has a maximum at $Q_z = 0$. From the value of $Q_{z,pk}^{hk}$ for the {11} peak, a tilt angle of $t = 29°$ with respect to the surface normal can be deduced. This angle decreases continuously on compressing the monolayer throughout the L_2 phase.

Going to phase L_2', the tilt azimuth changes to that of the next nearest neighbor, in the [10] direction. Hence both the (20) and {11} reflections exhibit a nonzero $Q_{z,pk}^{hk}$, but since the azimuths Ψ_{hk} are different so are the values of $Q_{z,pk}^{hk}$. The tilt angle $t = 15°$ is consistent with both measurements.

For the remaining three phases S, CS, and LS, the fact that all Q_z-scan maxima occur in the plane of the water surface ($Q_{z,pk}^{hk}$ = 0) indicates vertical chain orientation.

The surface area per chain A_t in a centered rectangular lattice

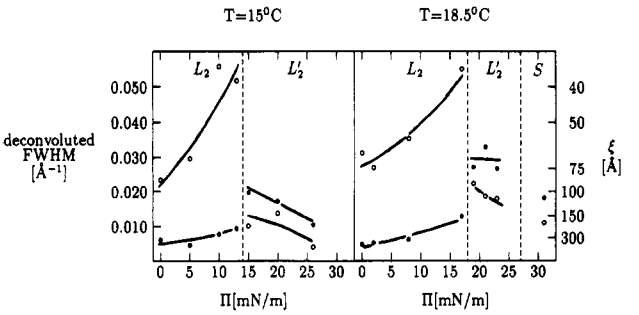

Figure 6. Deconvoluted peak width (fwhm) as a function of lateral pressure for a docosanoic acid monolayer at 18.5 and 15 °C. The open symbols correspond to the {11} peak and the full symbols to the {20} peak.

can be calculated from the measured lattice spacings by using the formula

$$A_t = \frac{2d_{20}^2 d_{11}}{(4d_{20}^2 - d_{11}^2)^{1/2}} \quad (4)$$

For a hexagonal lattice $d_{20} = d_{11} = d$ and eq 4 transforms into

$$A_t = 2d^2/3^{1/2} \quad (5)$$

To apply eqs 4 and 3, indices (h, k) have to be assigned properly to the measured spacings. For a packing with tilted molecules (phases L_2 and L_2'), incorrect assignment will result in inconsistent values of molecular tilt from eq 3. For a packing with upright molecules (phases CS and S), the {11} peak is twofold degenerate and is expected to show a larger integrated intensity than the nondegenerate (20) peak.

The values of surface area A_t derived from the diffraction measurements are shown in Figure 1 plotted against surface pressure and compared to the Π–A isotherms obtained more conventionally for 7 and 18 °C. Since the absolute value of A determined from the isotherms is less accurate than that measured by X-ray diffraction, the abscissa in the isotherms was normalized to give agreement of the two values for the highest pressure. It can be seen that the other values agree reasonably well. This supports our data analysis and in particular the assignment of the lattice orientations. In the specific case of the CS phase, the alternative assignment of peaks yields the unrealistically low value of 0.173 nm^2. It can also be seen that there are significant differences in the two-dimensional molecular density of the monolayer at different temperatures but identical surface pressures. From the areas A_t measured via the X-ray analysis it is possible to calculate a microscopic two-dimensional compressibility from the equation

$$\kappa_{2D} = -\frac{1}{A_t}\frac{\partial A_t}{\partial \Pi} \quad (6)$$

The value of κ_{2D} calculated from eq 6 for the L_2 phase is 8×10^{-3} m/mN and for the CS phase 3×10^{-4} m/mN, which is about the resolution limit of the experiment. It is remarkable that κ_{2D} of the CS phase is more than a factor of 2 smaller than the compressibility of phospholipid monolayers at high pressures,[18] when the monolayer is commonly said to be in the solid state. This should not be confused with the S phase characterized in the present work. The lipid molecules in the previous report[13,18] were vertical and hexagonally close packed, which is the arrangement now found in the LS phase.

In the L_2 phase there are large differences in the widths of the two Q_x-scan peaks, which indicates an anisotropy of positional correlation. To quantify this further, Figure 6 gives the peak width and the corresponding correlation length ξ as a function of surface pressure for two different temperatures where the L_2 and L_2' phases can exist. At low temperatures corresponding to the CS phase the line width is resolution limited. The data given in Figure 6 are not corrected for equipment resolution, so that the true line

(17) Kitaigorodskii, A. I. *Organic Chemical Crystallography*; Consultants Bureau: New York, 1961.

(18) Kjaer, K.; Als-Nielsen, J.; Helm, C. A.; Tippmann-Krayer, P.; Möhwald, H. *J. Phys. Chem.* **1989**, *93*, 3200.

width is somewhat smaller. Nevertheless they display several remarkable features:

1. Within the L_2 phase one line is a factor of 3–5 broader than the other one and its width increases with surface pressure.

2. In the L_2' phase the two widths are rather similar and smaller than that of the broad peak in the LS phase. Although there is scatter in the data, it can be seen that the width of the narrower line increases slightly on going from the L_2 to the L_2' phase.

The line-width anisotropy can be correlated with the tilt anisotropy. For the L_2 phase the narrow peak belongs to a family of lattice lines parallel to the tilt direction, i.e., $\Psi_{20} = 90°$, whereas the azimuth angle Ψ_{11} corresponding to the broad peak is approximately 30°. In the L_2' phase both Ψ_{11} and Ψ_{20} are nonzero, but again the larger azimuth corresponds to the family of lines with the broader peak. On compression, the tilt angle decreases, reducing the influence of tilt fluctuations, and this may be responsible for the decreasing line width. However, the latter argument also incorrectly predicts a decrease in line width with surface pressure in the L_2 phase, so that another unknown mechanism must be operative.

Discussion and Conclusions

The above results have confirmed previous isotherm measurements proving the multiplicity of phases in monolayers of the long chain fatty acids. We have observed a monomodal distribution of chain tilt that differs qualitatively between these phases.

Analysis of the isotherms of the long-chain fatty acids has shown qualitatively similar phase diagrams with transition temperatures increasing by 5–10 K on increasing the chain length by one methylene group.[15] Hence it is to be expected that the packings observed in the present experiments will also be found for other acids. In fact, the lattice structure and chain orientation basically agree with the results of Lin et al.[19] obtained from heneicosanoic acid, $C_{20}H_{41}COOH$, with one CH_2 less than docosanoic acid. We have not yet observed in diffraction the low-temperature low-surface-pressure phase labeled L_2'' by Lundquist[20] and B by Lin et al., although its high-temperature limit is evident as a double kink in the 7 °C isotherm of Figure 1. Conversely we have observed the LS phase not reported by Lin et al. Note that the description "centered rectangular"[22] for four of the present two-dimensional lattices is equivalent to the "distorted hexagonal" of refs 19 and 18. Similar phases have also been found by Schlossmann et al. for tetracosanic acid.[21]

The present results can also be compared to previous results of the present authors for eicosanoic (arachidic) acid[18] at ambient temperature. In conformity with isotherm studies, it is not surprising that only the L_2 and LS phases were observed, as the transitions to the L_2', S, and CS phases only occur at lower temperatures.

The fact that some of the phases are characterized by rather small values of positional correlation length supports the notion that many fatty acid monolayers exhibit mesophases.[20,23] A mesophase may be defined as one which displays the combination of long-range orientational order (meaning algebraic decay of orientational correlations) with short-range translational order (meaning geometric decay of translational correlations). The presence of long-range orientational order has been shown conclusively for the L_2 phase by using polarized fluorescence microscopy,[24] and indirectly for the L_2', LS, and S phases by using polarized microscopy to observe multilayer films deposited on solid substrates.[25] Hence it is reasonable to compare these phases to the usual categories of thermotropic liquid crystals.[26] Phases L_2, L_2', S, and LS show exactly the same unit cell symmetries as the smectic phases I, F, E, and B, respectively, and comparable diffuse diffraction patterns. This correspondence indicates that the wealth of thermotropic liquid crystal phases may be rediscovered for surfactant monolayers in the near future.

We should also note that there are similarities of these phases with 3D phases of long chain alkanes.[14,27] For the latter substances, crystalline but conformationally disordered phases have been observed. These display long-range translational order, but, for example, in the so-called rotator phases the chain is free to rotate around its long axis and occupies a cross section greater than 0.19 nm^2. In the ordered crystalline phases, on the other hand, the cross section is less than 0.19 nm^2 and cannot be considered circular since the rotation is frozen in. The surface area A_t and the cross-sectional area A_c normal to the molecular axis are related to the tilt angle t by simple geometry according to

$$A_t = A_c/\cos t \tag{7}$$

For the examples in Figures 4 and 5 where Q_z-resolved rod scans are displayed, we derive A_c to be 0.197, 0.192, 0.192, 0.192, and 0.187 nm^2 for the LS, L_2, L_2', S, and CS phases, respectively. A_c is constant (± 0.001 nm^2) within each phase. Hence molecular rotation is definitely possible in the LS phase, but not in the CS phase. For L_2, L_2', and S the situation is intermediate, and therefore a restricted rotation around the long axis may be possible.

These differences of molecular cross section imply differences in the three-dimensional electron density between phases. We have previously shown that the electron density changes by less than 1% within one phase.[18] Hence the transitions $L_2' \rightarrow$ LS, LS $\rightarrow$ S, S $\rightarrow$ CS, $L_2' \rightarrow$ CS, and $L_2 \rightarrow$ CS involve discontinuities in the density, as expected for first-order phase transitions and as consistent with the assignment of transition order by Ställberg-Stenhagen and Stenhagen.[16]

The positional correlation length was found to be anisotropic, being up to 5 times smaller along the tilt direction than perpendicular to it. This does not prove but supports the picture of a modulated structure where the monolayer consists of stripes of uniform tilt, which extend on the order of 10 spacings parallel to the tilt direction but 100 spacings perpendicular to it. Such stripes and two-dimensional micelles have been discussed in connection with molecular dynamics and Monte Carlo simulations.[28,29] The observed behavior can also be derived from a model with independent fluctuations of molecular position and orientation. This leads to a reflection width which increases with Q_z.[34]

Langmuir–Blodgett films are usually prepared with divalent ions in the subphase.[30] Their presence drastically influences isotherms, and hence also the Π–T phase diagram. It is conceivable that this may transform a film into the CS phase or suppress the L_2 phase. The energetics of film transfer onto a solid support very likely depends on its phase on the water surface. We suggest that it will be fruitful to investigate the influence of ions on monolayer phases.[35]

It is of interest to note that the phases L_2 and L_2' were found to be important for reducing the level of orientational defects in 22-tricosenoic acid monolayers. Defect elimination was only observed when the monolayer was cycled between the two.[31] The present results provide a molecular basis for the efficiency of this annealing process. The defects are related to the tilt azimuth, which changes discontinuously with respect to the crystalline lattice as the transition occurs. Enhanced molecular mobility could result from the weakening of restoring forces near a phase transition.

(19) Lin, B.; Shih, M. C.; Bohanon, T. M.; Ice, G. E.; Dutta, P. *Phys. Rev. Lett.* **1990**, *65*, 191.
(20) Lundquist, M. *Chem. Scr.* **1971**, *1*, 5, 207.
(21) Schlossmann, M. L.; Schwartz, D. K.; Pershan, P. S.; Kawamoto, E. H.; Kellog, G. J.; Lee, S. *Phys. Rev. Lett.*, submitted for publication.
(22) *International Tables for Crystallography*; Hahn, Theo, Ed.; D. Reidel: Dordrecht, 1987.
(23) Peterson, I. R.; Earls, J. D.; Girling, I. R.; Russell, G. J. *Mol. Cryst. Liq. Cryst.* **1987**, *147*, 141.
(24) Moy, V. T.; Keller, D. J.; Gaub, H. E.; McConnell, H. M. *J. Phys. Chem.* **1986**, *90*, 3198.
(25) Veale, G.; Girling, I. R.; Peterson, I. R. *Thin Solid Films* **1985**, *127*, 293.
(26) Gray, G. W.; Goodby, J. W. *Smectic Liquid Crystals: Textures and Structures*; Leonard Hill: Glasgow, 1984.
(27) Doucet, J.; Denicol, I.; Craievich, A. F.; Germain, C. *J. Chem. Phys.* **1984**, *80*, 1647.
(28) Saffran, S. A.; Robbins, M. O.; Garoff, S. *Phys. Rev.* **1987**, *A33*, 2186.
(29) Binder, K.; Landau, D. P. In *Advances in Chemical Physics*; Kawley, K. P., Ed.; Wiley: New York, 1989; p 91.
(30) Kuhn, H.; Möbius, D.; Bücher, H. In *Physical Methods of Chemistry*; Weisberger, A., Rossiter, B., Eds.; Wiley: New York, 1972; Vol. 1, Part 3B.
(31) Bibo, A. M.; Peterson, I. R. *Thin Solid Films* **1987**, *178*, 81.

The consequent higher density of thermally excited translational defects may be a reason for the line-width maximum near the transition pressure of 18 mN/m in Figure 6.

The present series of phase changes may explain the finding of surface roughness decreasing with the application of surface pressure.[32] This contrasts with the finding for fatty acids or phospholipids in less condensed states where the decreased surface tension on compression leads to a larger amplitude of surface capillary waves.[33] In the case of more ordered monolayer states there may be an additional elastic force flattening the surface. Unfortunately the isotherm given in ref 32 differs considerably from those of Figure 1, and it is not possible to identify the corresponding phase regions with certainty.

This work has confirmed the existence of a rich polymorphism in fatty acid monolayers and demonstrated qualitative differences of symmetry between phases. To do this we have analyzed our data in terms of a crystalline model of film organization, assuming that the peaks of scattered intensity occur at the same positions as they would from a defect-free lattice. We have acknowledged departures from perfect crystallinity by deriving decay lengths of translational correlation from the peak widths. However, it is clear that the precise details of our scattered intensity profile data contain far more information and demand a more detailed analysis. This is presently under way. We hope to extract information on more subtle but nevertheless very important differences between these phases, which may even result in further refinement of the phase diagram. It is ironic that, hitherto, these compounds were considered to be so simple as to be of little interest.

Acknowledgment. Thanks are due to the staff at HASYLAB for ample beam time and support. This work was funded by the Bundesministerium für Forschung und Technologie (BMFT), the Deutsche Forschungsgemeinschaft (SFB262), the Materialwissenschaftliche Forschungszentrum (MWFZ) of the Universität Mainz, the Fonds der Chemischen Industrie, and the Danish Natural Science Foundation.

(32) Daillant, J.; Bosio, L.; Benattar, J. J.; Meunier, J. *Europhys. Lett.* **1989**, *8*, 453.
(33) Helm, C. A. Ph.D. Thesis, Physics Faculty, T.U. München, 1988.
(34) Peterson, I. R. To be published.
(35) Leveiller, F.; Jacquemain, D.; Lahav, M.; Leiterowitz, L.; Deutsch, M.; Kjaer, K.; Als-Nielsen, J. *Science*, submitted for publication.